Supporting Information

Tailoring optoelectronic properties and dielectric profile of few-layers S-doped

MoO$_3$ and O-doped MoS$_2$ nanosheets: a first-principles study

Masoud Shahrokhi [1,2], Tangui Le Bahers [1], and Pascal Raybaud[1,2,*]

[1]*Univ Lyon, ENS de Lyon, CNRS, Université Claude Bernard Lyon 1,*
Laboratoire de Chimie UMR 5182, F-69342 Lyon, France
[2]*IFP Energies nouvelles, Rond-point de l'échangeur de Solaize, BP 3, 69360 Solaize, France*

Corresponding author: pascal.raybaud@ifpen.fr

S1. Optoelectronic properties of non-doped 4L MoO₃ and O-doped 6L MoS₂
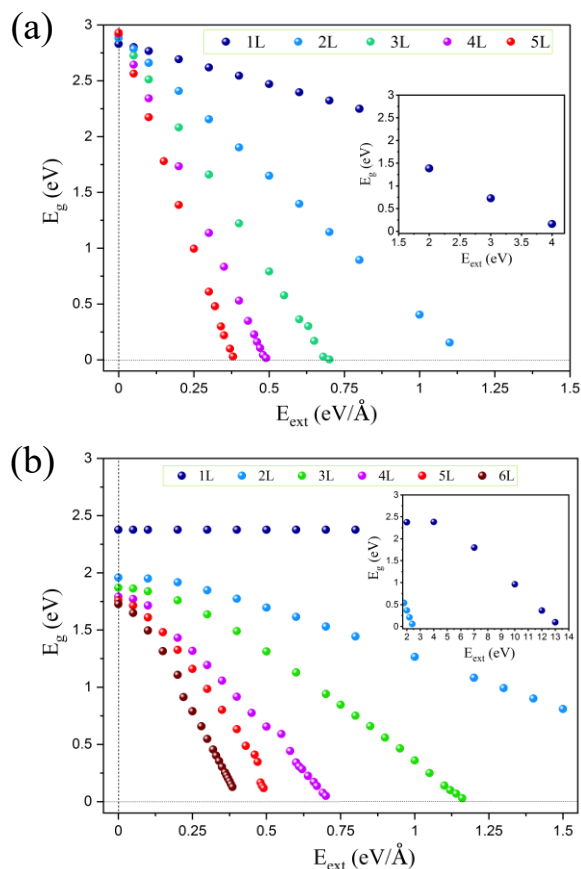

Figure S1. Calculated electronic band gap as a function of external electric field (E_{ext}) along out-of-plane direction for 1L-5L MoO₃ (a) and 1L-6L MoS₂ (b) within HSE06. Insets show the electronic band gap of FL MoO₃ and MoS₂ as a function of strong electric field (E_{ext} > 1.5 eV/Å).

The electronic band gap of MoO_3 and MoS_2 multilayers shows a monotonous decrease with increasing external electric field. Whereas the band gap of single-layer structures slightly decreases for electric field from 0 eV/Å to 1 eV/Å, it reduces drastically by applying stronger electric fields E_{ext} > 2 eV/Å for SL MoO_3 and E_{ext} > 7 eV/Å for SL MoS_2.

As explained in Refs.[1,2], the initial step of the microscopic dielectric profile calculation is a study of the variation of the total induced dipole (m_z) of multilayer MoO_3 and MoS_2 systems as a function of the number of layers. According to Refs.[1,2], it is expected that only for small external electric field, the

induced dipole have a linear variation as a function of E_{ext}. The slope of the inverse dipole variation as a function of 1/L (L is array period between two layered slabs), is equal to $1/(\varepsilon_0.E_{ext})$.
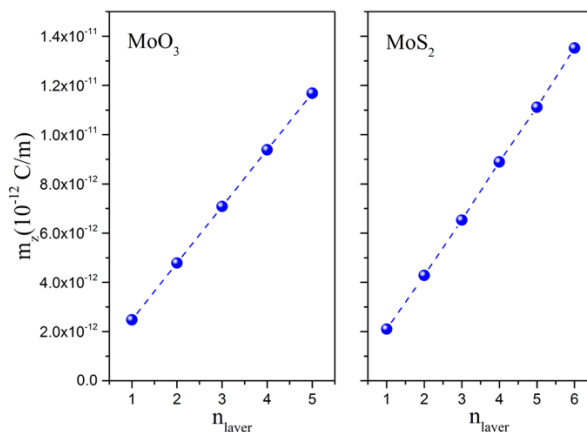
Figure S2. Variation of the induced dipole m_z for pristine MoO₃ and MoS₂ layered structures with increasing number of layers. The external electric field is $E_{ext} =0.025$ eV/Å.
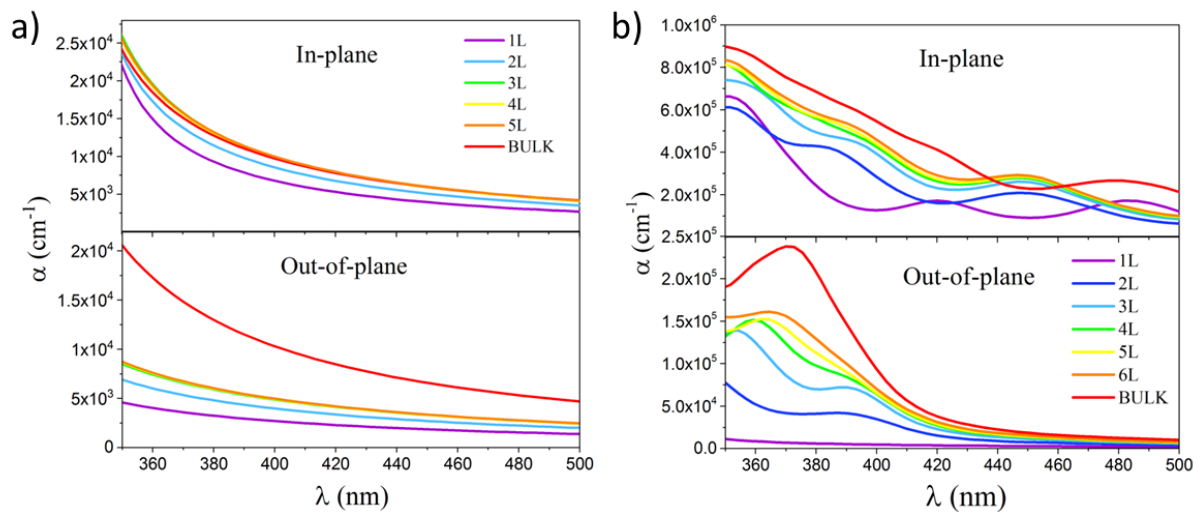
Figure S3. Computed absorption coefficients (α, in cm^{-1}) along in-plane and out-of-plane for a) 1L-5L and bulk MoO₃ and b) 1L-6L and bulk MoS₂ (right panel) within HSE06 approach.

S2. S-doped 4L MoO_3 and O-doped 6L MoS_2

S2.1. Structural properties

S concentration (%)	System	corresponding cell	corresponding figure	k-point mesh	a (Å)	b (Å)	T (Å)	E_b (eV)	E_g (eV)	ε_{eff}
0.0	MoO_3	unit cell	Fig. S5 (a)	12×12×1	3.712	3.934	27.315	-8.00	2.92	3.60
4.16 (bulk)	$MoS_{0.12}O_{2.88}$	unit cell	Fig. S5 (b)	12×12×1	3.714	3.928	28.675	-7.72	1.48	4.08
4.16 (edge)	$MoS_{0.12}O_{2.88}$	unit cell	Fig. S5 (c)	12×12×1	3.714	3.930	27.737	-7.75	2.18	3.96
8.33 (bulk-configure-1)	$MoS_{0.25}O_{2.75}$	unit cell	Fig. S5 (d)	12×12×1	3.715	3.933	29.342	-7.46	1.86	4.99
8.33 (bulk-configure-2)	$MoS_{0.25}O_{2.75}$	unit cell	Fig. S5 (e)	12×12×1	3.716	3.924	30.00	-7.43	1.46	5.14
8.33 (bulk-configure-3)	$MoS_{0.25}O_{2.75}$	unit cell	Fig. S5 (f)	12×12×1	3.716	3.925	29.92	-7.44	1.46	5.15
8.33 (edge)	$MoS_{0.25}O_{2.75}$	unit cell	Fig. S5 (g)	12×12×1	3.716	3.925	28.166	-7.49	2.16	4.15
16.66 (bulk)	$MoS_{0.5}O_{2.5}$	unit cell	Fig. S5 (h)	12×12×1	3.713	3.934	29.52	-6.88	0.00	-----
16.66 (edge-pre-edge-configure-1)	$MoS_{0.5}O_{2.5}$	unit cell	Fig. S5 (i)	12×12×1	3.72	3.898	31.10	-6.92	0.65	5.65
16.66 (bulk-edge-configure-2)	$MoS_{0.5}O_{2.5}$	unit cell	Fig. S5 (j)	12×12×1	3.719	3.921	30.261	-6.94	1.85	5.32
25	$MoS_{0.75}O_{2.25}$	unit cell	Fig. S5 (k)	12×12×1	3.723	3.916	32.821	-6.38	1.44	5.93
33	$MoSO_2$	unit cell	Fig. S5 (l)	12×12×1	3.724	3.922	34.306	-5.86	1.86	7.51

Table S1. Different models, corresponding figures, *k*-point mesh, calculated optimized lattice parameters (*a* and *b*), calculated the layer thickness (*T*), binding energy (*E_b*) per MoO_3, the electronic band gap (E_g) and effective high frequency dielectric constant (ε_{eff}) along out-of-plane direction for the S-substituted 4L MoO_3 for different concentrations.
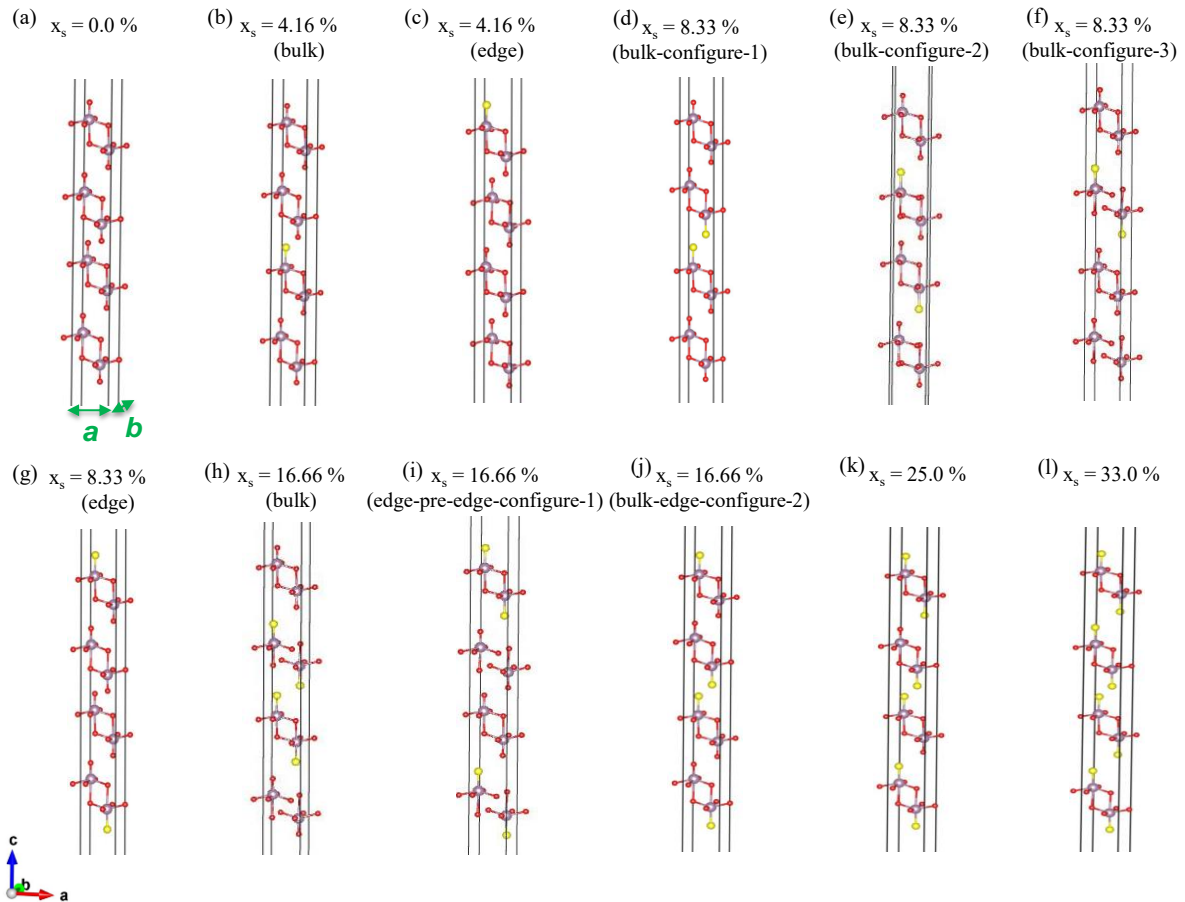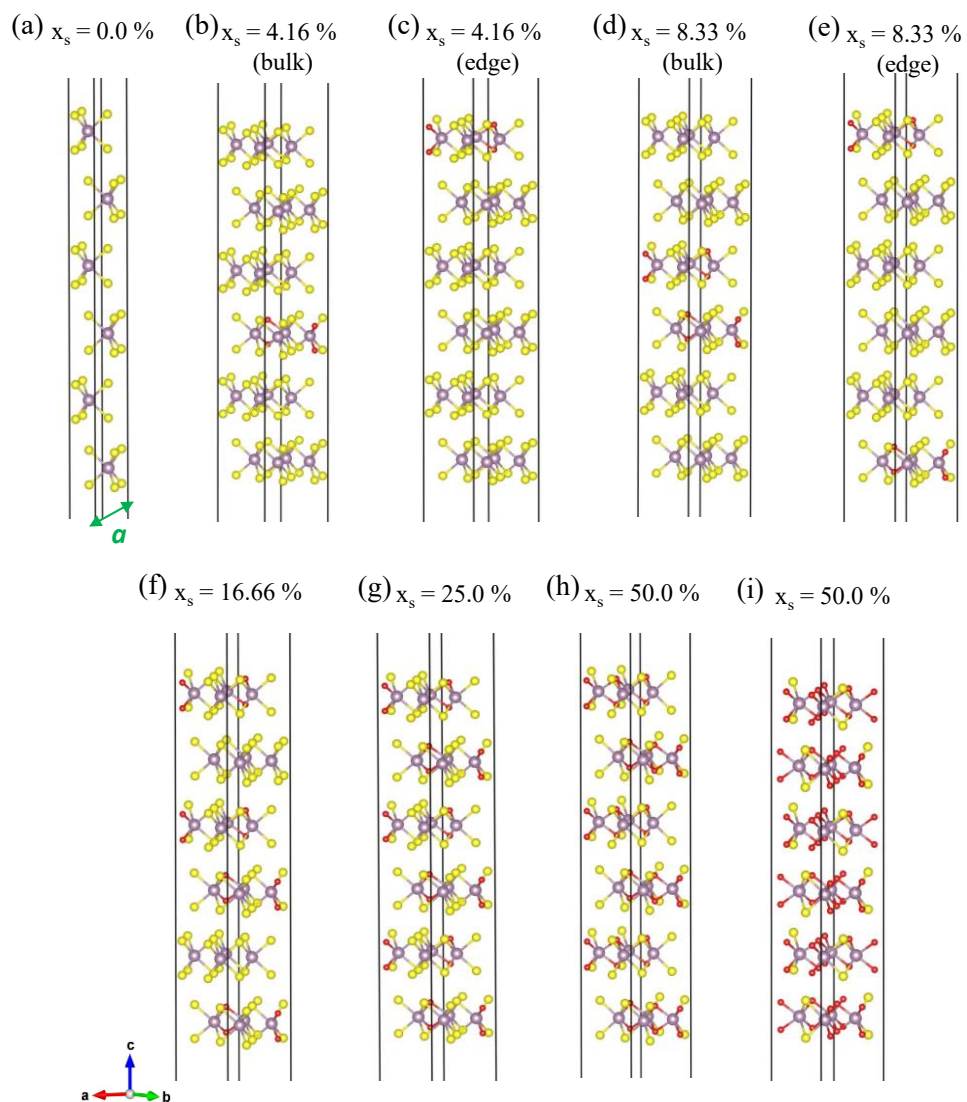
Figure S4. Optimized structures of S-doped 4L MoO₃ for different concentrations. The purple, red and yellow balls in the geometrical models represent the Mo, O and S atoms, respectively. The lattice parameters of pristine structure are also shown with green arrows.

O concentration (%)	System	corresponding cell	corresponding figure	*k-point mesh*	*a* (Å)	*T* (Å)	E_b (eV)	E_g (eV)	ε_{eff}
0.0	MoS_2	unit cell	Fig. S6 (a)	12×12×1	3.156	33.860	-2.250	1.73	6.26
4.16 (bulk)	$MoO_{0.08}S_{1.92}$	(2 × 2)	Fig. S6 (b)	6×6×1	3.141	33.837	-2.349	1.21	6.14
4.16 (edge)	$MoO_{0.08}S_{1.92}$	(2 × 2)	Fig. S6 (c)	6×6×1	3.141	33.855	-2.353	1.27	6.22
8.33 (bulk)	$MoO_{0.17}S_{1.83}$	(2 × 2)	Fig. S6 (d)	6×6×1	3.125	33.810	-2.453	1.27	6.00
8.33 (edge)	$MoO_{0.17}S_{1.83}$	(2 × 2)	Fig. S6 (e)	6×6×1	3.125	33.889	-2.458	1.38	6.13
16.66	$MoO_{0.33}S_{1.67}$	(2 × 2)	Fig. S6 (f)	6×6×1	3.095	33.879	-2.681	1.48	5.77
25	$MoO_{0.5}S_{1.5}$	(2 × 2)	Fig. S6 (g)	6×6×1	3.065	33.845	-2.923	1.62	5.35
50	$MoOS$	(2 × 2)	Fig. S6 (h)	6×6×1	2.980	33.835	-3.661	1.75	4.44
75	$MoO_{1.5}S_{0.5}$	(2 × 2)	Fig. S6 (i)	6×6×1	2.890	31.290	-4.482	1.54	3.78

Table S2. Different models, corresponding figures, *k*-point mesh, calculated optimized lattice parameter (*a*), calculated the layer thickness (*T*), binding energy (E_b) per MoS₂, the electronic band gap (E_g) and effective high frequency dielectric constant (ε_{eff}) along out-of-plane direction for the O-substituted 6L MoS₂ for different concentrations.

(a) $x_s = 0.0\%$

(b) $x_s = 4.16\%$ (bulk)

(c) $x_s = 4.16\%$ (edge)

(d) $x_s = 8.33\%$ (bulk)

(e) $x_s = 8.33\%$ (edge)

(f) $x_s = 16.66\%$

(g) $x_s = 25.0\%$

(h) $x_s = 50.0\%$

(i) $x_s = 50.0\%$

Figure S5. Optimized structures of O-doped 6L MoO₃ for different concentrations. The purple, red and yellow balls in the geometrical models represent the Mo, O and S atoms, respectively. The lattice parameters of pristine structure are also shown with green arrows.

S2.2 Energetics and thermodynamic analysis

To evaluate the energetics of S-doped 4L MoO_3 structures, the binding energies (E_b) normalized per MoO_3 were computed as

$$E_b = \frac{E_{tot} - \left(n_{Mo}E_{Mo} + \left(\frac{1}{2}\right)n_O E_{O_2} + n_S E_{S_\alpha}\right)}{N/4} \quad (1)$$

and the binding energies of O-doped 6L MoS_2 structures normalized per MoS_2 were computed as

$$E_b = \frac{E_{tot} - \left(n_{Mo}E_{Mo} + n_S E_{S_\alpha} + \left(\frac{1}{2}\right)n_O E_{O_2}\right)}{N/3} \quad (2)$$

where E_{tot} is the total energy per cell, E_i is the energy of the i-th individual elements in their respective ground states, n_i is the number of species i in the structure and $N/4$ and $N/3$ are the number of MoO_3 and MoS_2 per unit cell.

However, the binding energy cannot discriminate the relative stability of structures with various chemical compositions. Hence, to determine the thermodynamic stability of 4L $MoO_{3-x}S_x$ and 6L $MoS_{2-x}O_x$ compositions as a function of the number of S- or O-atoms exchanged in the 4L MoO_3 and 6L MoS_2 layered structures respectively, we calculate the Grand potential, Ω, assuming that the reservoir surrounding the solids is constituted from ideal gas phase mixtures of H_2S/H_2O (commonly used experimentally as sulfiding and oxidizing agents):

4L MoO_3 + xH_2S = 4L $MoO_{(3-x)}S_x$ + xH_2O (3)

6L MoS_2 + xH_2O = 6L $MoS_{(2-x)}O_x$ + xH_2S (4)

$$\Omega_{MoO_{3-x}S_x} = E_b(4L\ MoO_{3-x}S_x) - E_b(4L\ MoO_3) + xG^0_{f,T_0}(H_2O) - xG^0_{f,T_0}(H_2S) - xRT_0\ln\left[\frac{p(H_2S)}{p(H_2O)}\right]$$

(5)

$$\Omega_{MoS_{2-x}O_x} = E_b(6L\ MoS_{2-x}O_x) - E_b(6L\ MoS_2) + xG^0_{f,T_0}(H_2S) - xG^0_{f,T_0}(H_2O) - xRT_0\ln\left[\frac{p(H_2O)}{p(H_2S)}\right] (6)$$

where E_b stands for the 0 K, binding energies of the different solids involved (neglecting vibrational and entropic contributions, see also supporting information), G^0_{f,T_0} stands for the Gibbs free energies of formation of H_2S and H_2O molecules (including thermal and entropic effects evaluated from NIST data base at T_0=298 K). So, for each value of x, we will plot the evolution of Ω_x as a function of the variable $\pm RT_0\ln\left[\frac{p(H_2O)}{p(H_2S)}\right]$ fixing the partial pressures of H_2S/H_2O in the reservoir assumed at T_0=298 K. It is worth to note that increasing T slightly diminishes (increases, respectively) the free enthalpy of oxidation (sulfidation, respectively) reaction. However, the main trends reported at ambient T are only very weakly affected.
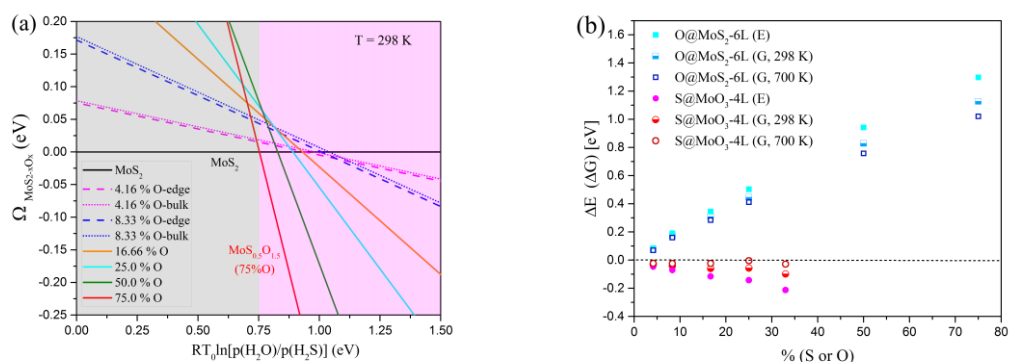
For the more discerning of the stability of these structures, we calculated the reaction energies for the most stable S-substituted 4L MoO_3 and O-substituted 6L MoS_2 nanostructures for different concentrations by using equations S3 and S4 as depicted in Fig 4. In this figure, ΔE is the difference of

0K binding energy of the S-substituted 4L MoO_3 and O-substituted 6L MoS_2 systems with respect to DFT binding energies of H_2S and H_2O as reactants/products:

$$\Delta E = E_b(4L\ MoO_{3-x}S_x) - E_b(4L\ MoO_3) + xE_b(H_2O) - xE_b(H_2S) \quad (7)$$

ΔG is the difference of binding energy of the S-substituted 4L MoO_3 and O-substituted 6L MoS_2 systems with respect to experimental free energies (enthalpy and entropy) of H_2S and H_2O given by NIST thermodynamic database:

$$\Delta G = E_b(4L\ MoO_{3-x}S_x) - E_b(4L\ MoO_3) + xG_b(H_2O) - xG_b(H_2S) \quad (8)$$
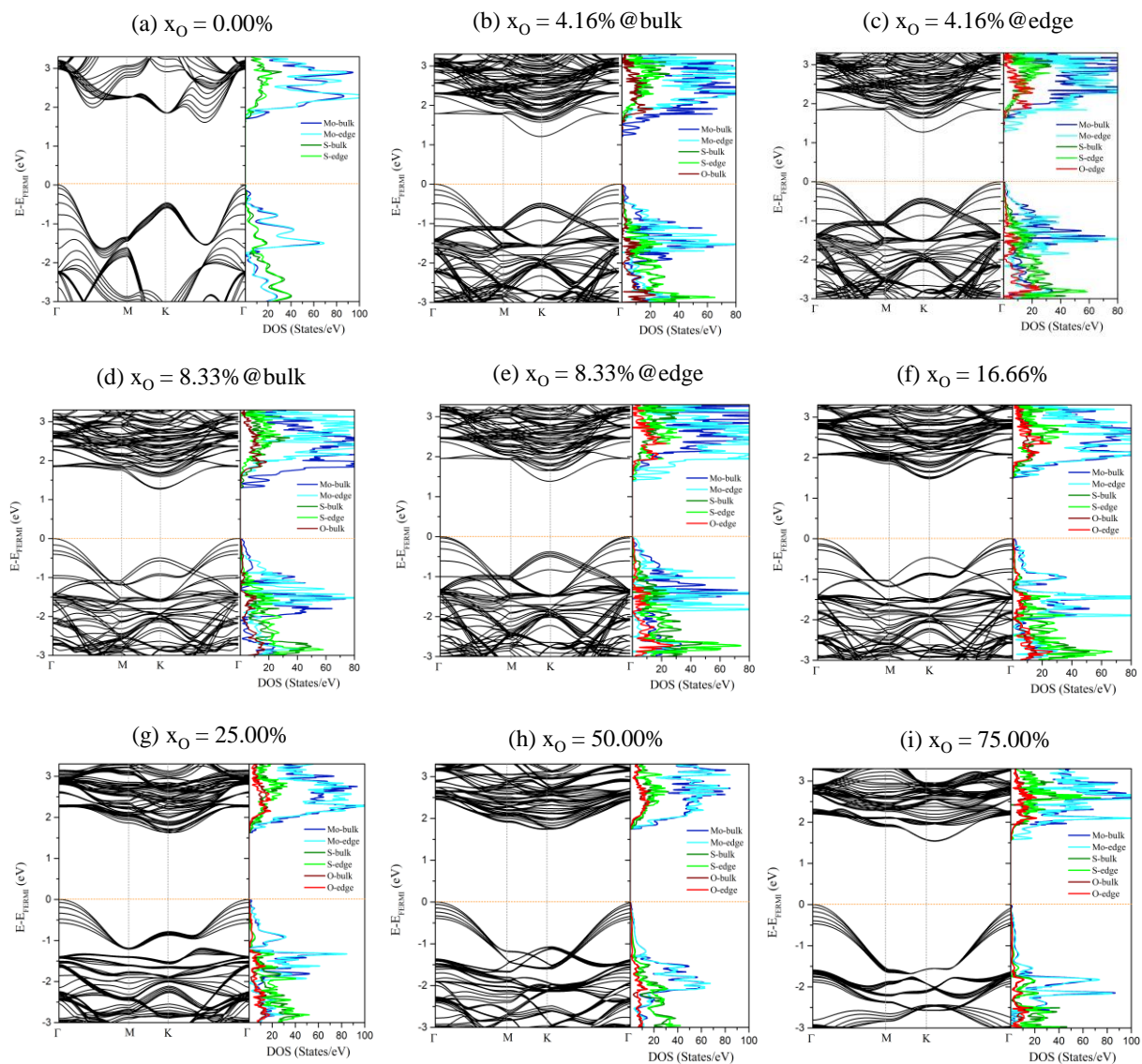

Figure S6. Thermodynamic phase stability of the O-substituted 6L MoS_2 (a) structures for different S- and O-concentrations with respect to pristine structures considering the H_2S/H_2O reservoir. The dashed and doted lines denote the results for impurity-substituted only in the edge and bulk of layered systems, respectively. (b) The calculated reaction energy for the most stable S-substituted 4L MoO_3 and O-substituted 6L MoS_2 structures for different concentrations.

S2.3 Electronic structure
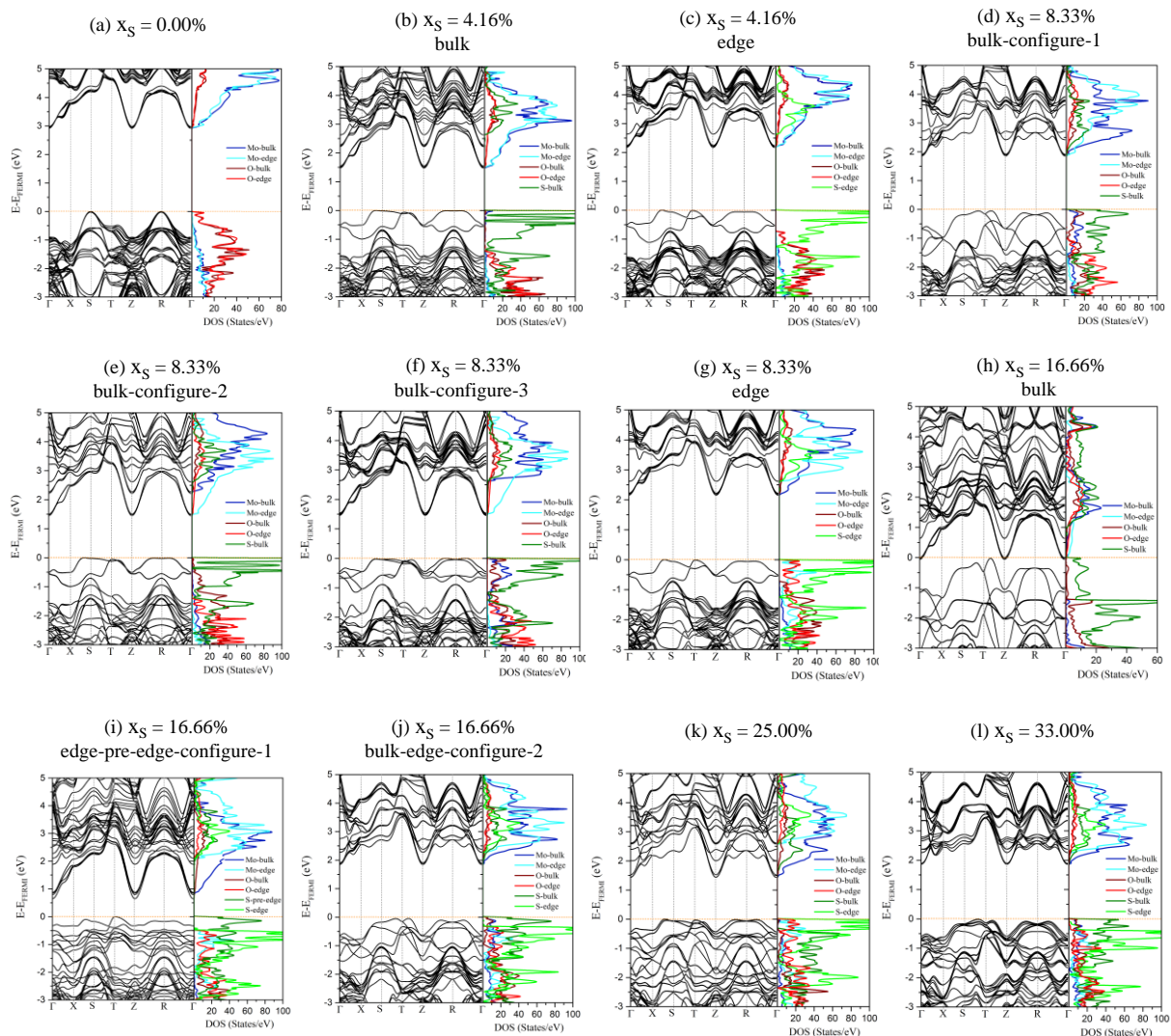
Figure S7. Band structure and PDOS of the most stable S-substituted 4L MoO₃ structures for different concentrations calculated using HSE06. The Fermi level is set to zero. The related structures are presented in Figure S4.

(a) $x_O = 0.00\%$

(b) $x_O = 4.16\%$@bulk

(c) $x_O = 4.16\%$@edge

(d) $x_O = 8.33\%$@bulk

(e) $x_O = 8.33\%$@edge

(f) $x_O = 16.66\%$

(g) $x_O = 25.00\%$

(h) $x_O = 50.00\%$

(i) $x_O = 75.00\%$

Figure S8. Band structure and PDOS of the most stable O-substituted 6L MoS$_2$ structures for different concentrations calculated using HSE06. The Fermi level is set to zero. The related structures are presented in Figure S5.

References

1 J. Even, L. Pedesseau and M. Kepenekian, Electronic surface states and dielectric self-energy profiles in colloidal nanoscale platelets of CdSe, *Phys. Chem. Chem. Phys.*, 2014, **16**, 25182–25190.

2 F. Giustino, P. Umari and A. Pasquarello, Dielectric Discontinuity at Interfaces in the Atomic-Scale Limit: Permittivity of Ultrathin Oxide Films on Silicon, *Phys. Rev. Lett.*, 2003, **91**, 267601.